Journal of Sustainable Energy & Environment

12 (2021) 77-85

Satellite precipitation characteristics and effects of land cover change in Greater Bangkok

Peerapol Chankasem[1,2], Kasemsan Manomaiphiboon[1,2*], Bikash Devkota[1,2], Hoang Thi Trang[1,2], Nitchanan Nantawong[1,2], Chakrit Chotamonsak[3] and Agapol Junpen[1,2]

[1]The Joint Graduate School of Energy and Environment, King Mongkut's University of Technology Thonburi, Thailand
[2]Center of Excellence on Energy Technology and Environment, Ministry of Higher Education, Science, Research, and Innovation, Thailand
[3]Department of Geography, Chiang Mai University, Thailand
*Corresponding author: kasemsan.jgsee@gmail.com, Tel.: +66 2 470–7331

Abstract: This study investigated a number of precipitation characteristics in Greater Bangkok (GBK) using hourly satellite–derived GPM (Global Precipitation Measurement) precipitation data for a period of 2001–2018 (as seasonal years). Long–term land cover and meteorological data were used to support the assessment. GPM well captures seasonality, with two peaks in the early and late wet season. On a diurnal scale, summer precipitation tends to occur during the afternoon and evening, so does wet–season precipitation with extension to the early morning hours. Spatial correlation analysis using the hourly data shows GBK as a homogeneous or coherent region of precipitation. Urban precipitation tends to be more intense and less distributed than its non–urban counterpart, suggesting that urban surface and city activities possibly enhance convection. Summer precipitation shows strong directional dependence, consistent with the prevailing surface and upper winds. As for urbanization effects, it was examined using a set of Hovmoller diagrams and normalized precipitation in the urban and non–urban areas between two epochs (2001–2009 and 2010–2018). March–May was found to have relatively large changes in magnitude than those in the other months. During the summer, such changes tend to occur mostly in the afternoon and evening/nighttime. Given the scope of the current investigation, it is still not possible to conclude whether urbanization induces more or less precipitation for the study area.

Keywords: Satellite, precipitation, gauge, urbanization, convection.

1. Introduction

Precipitation plays an important role in the system of climate and is a fundamental component of the hydrological cycle [1], providing freshwater resources for human activities and sustaining ecological systems. Knowledge and understanding of precipitation through research enable water resources to be managed properly [2–5]. A large city (or urban area) is generally populated and a center of human and economic activities, and has substantial built–up or artificial structures within (e.g., houses, buildings, and dense transportation networks). These cause urban surface to be rougher than that of its rural or less–urbanized surroundings, directly affecting wind flows over and within the city [6-7]. Artificial objects and a less–vegetative landscape typically have larger thermal inertia, thus storing more heat and longer before release back to the atmosphere. This results in an urban heat island phenomenon where urban temperature is higher than rural temperature for both air and land surface [8-9]. Additional heat emitted from various sources (mostly, fuel combustion in transportation, residential, commercial, and industrial sectors) modifies surface energy balance and strengthen urban heat island [8]. Air pollutants are also emitted in a relatively large amount. It is well known that aerosols (airborne particulate matter) can act as cloud condensation nuclei (CCN) [3, 6]. Some aerosols absorb or scatter incoming solar radiation, depending on types. These are inevitably involved with convective and cloud processes over the city and its vicinity and inevitably modify precipitation patterns (in terms of magnitude, frequency, duration, timing, and location) [3, 10-12].

Traditionally, precipitation is measured by a gauge. Not all areas have gauges available to observe precipitation sufficiently. Other techniques of precipitation measurement have been available, especially, weather radar and satellite remote sensing. Ground–based radar gives information of precipitation and its movement at relatively high spatial and temporal resolutions but the accuracy of detection is subject to instrument, signal, and atmospheric conditions, as well as ground clutter. Satellite precipitation is essentially derived from space–based remote sensing and developed algorithms. Detections by individual sensors onboard multiple satellites can also be incorporated or merged into an advanced data processing that generates satellite precipitation estimates (quasi)–globally with relatively high spatial and temporal resolutions. Satellite precipitation data are nowadays widely distributed and used by not only scientific research, weather or hydro–meteorological operations but also the general public. Many satellite precipitation products are available and accessible [13-14]. Trang et al. [15] intensively evaluated the prediction capability of seven products and suggested Global Precipitation Measurement (GPM) [16-17] as a reasonably performing product.

This study investigated a number of precipitation characteristics and potential urbanization impacts for Greater Bangkok (GBK) (Figure 1) and utilized GPM for long–term precipitation data for the investigation. GBK is the largest urban agglomeration in Thailand, comprising the following six provinces: Bangkok (the capital), Nakhon Pathom, Nonthaburi, Pathumthani, Samut Prakan, and Samut Sakhon. The study hopes to demonstrate the applicability of satellite precipitation for a large urban area and to seek a scientific evidence as to whether

continuous urbanization in GBK over the recent two decades has modified urban precipitation. To our knowledge, urban climate research conducted for GBK has focused mostly on temperature, [e.g., 8-9, 18] but limited to other variables, precipitation [19-20], and wind [7]. Some findings from this study can supplement the current knowledge of precipitation characteristics in the study area.

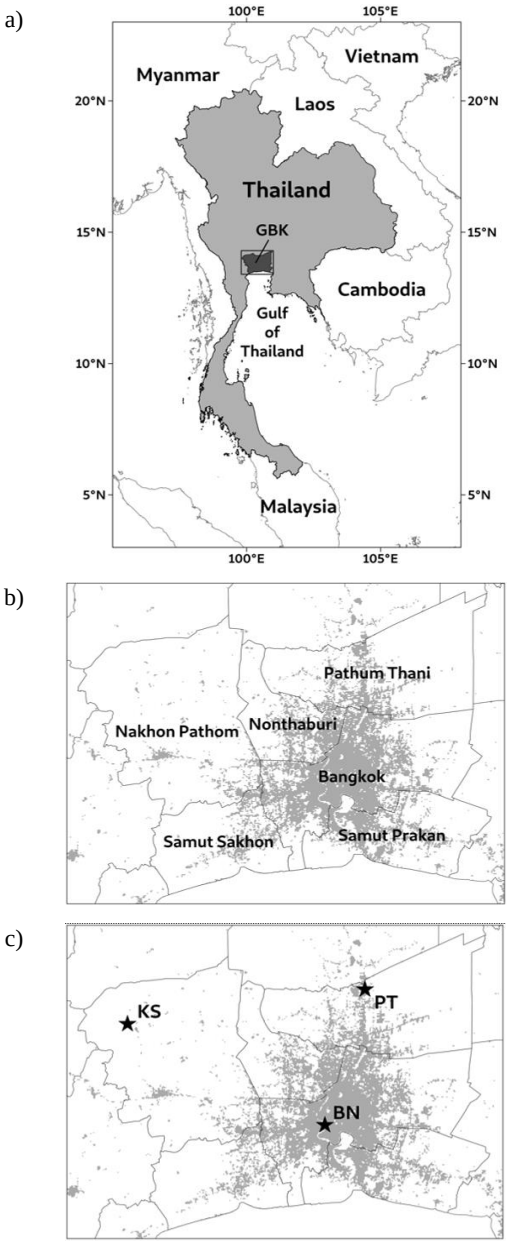

Figure 1. a) Thailand, b) Greater Bangkok and its six provinces, and c) gauges considered. The grey shading indicates built–up areas.

2. Study Area

The study area focused here is GBK, which is situated within the central plain of Thailand. It has continuous population and economic growths and urbanization after the year 2000 (Figure 2). The growth rates of registered population and urbanization in GBK are obviously faster than those in Bangkok. However, total energy consumption in each of GBK and Bangkok does not have a relative change as much as that for the country. Urbanization has continuously increased, with a faster rate seen in GBK than in Bangkok.

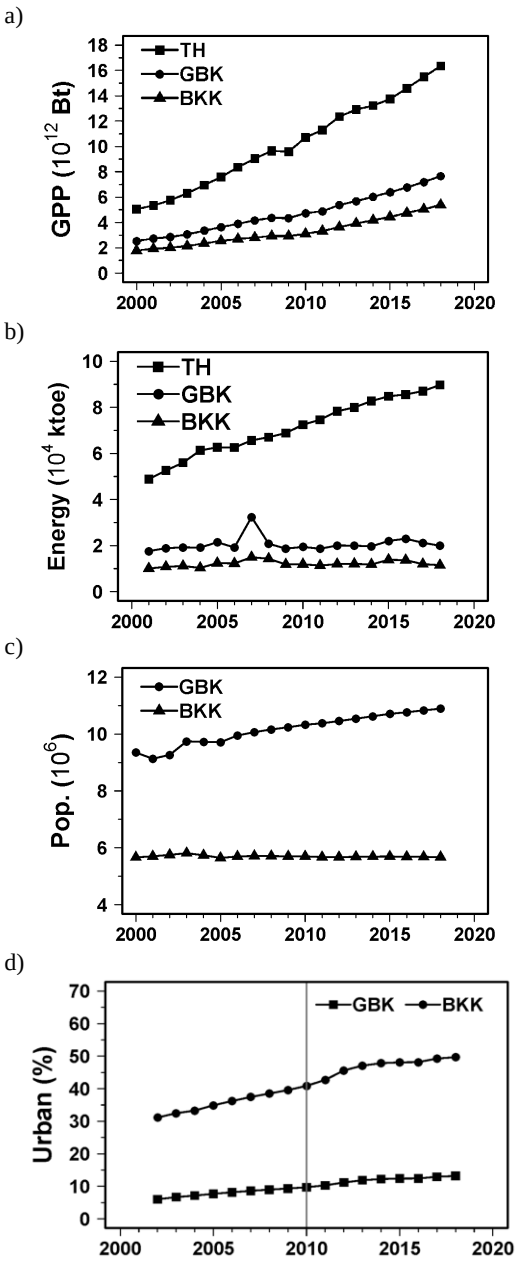

Figure 2. a) Gross provincial product (GPP) (at current market price) [24], b) energy consumption (in units of 104 ktoe and 1 ktoe = 41,868 × 109 J) [25], c) registered population [26], and d) total urban area (%) [27]. GPP has the same definition as the national gross domestic product (GDP) but scaled to a provincial level instead. The acronyms TH, GBK, and BKK stand for Thailand, Greater Bangkok, and Bangkok, respectively.

The general climate of GBK is similar to the upper part of Thailand, which are seasonally divided into winter, summer, and wet (or rainy) seasons [21-22]. The winter has dry and cool weather with no or limited rain influenced by the regional northeast monsoon and lasts from November to February. The summer coincides with the transition of the two monsoonal periods (northeast to southwest) and lasts two months (March–April) with warm and more humid weather. April is usually the warmest month. In this season, thunderstorms with strong winds and abrupt intense rainfalls occur occasionally, and persistent southerly wind from the Gulf of Thailand brings moisture inland. The wet season is influenced by the southwest monsoon, carrying plenty of moisture from the Indian Ocean and the Gulf of Thailand and resulting in substantial rain in most of the country. The wet

season lasts from May to October. In Upper Thailand and GBK, precipitation has two peaks during the early and late wet season, caused by the meridional migration of the Intertropical Convergence Zone (ITCZ) (or called the monsoon trough).

3. Data and Methods

3.1 Gauge data

To evaluate satellite precipitation estimates, data from selected standard (i.e., manual) gauges and automatic gauges of the Thai Meteorological Department (TMD) (see Figure S1 in Supplementary Materials for example) were obtained from selected three weather stations (Figure 1c and Table 1). The standard–gauge (SG) data have 3–hourly accumulated samplings reported at 1, 4, 7, 10, 13, 16, 19, and 22 LT (local time) (LT = UTC + 7). The automatic–gauge (AWS) data are available directly at http://www.aws–observation.tmd.go.th/web/main/index.asp) [23]. Precipitation is measured from an automatic weather system located within each of the three stations. Here, 10–min data were downloaded and combined to form hourly data. In fact, there are more than three stations of the TMD located within GBK but those with a large amount of missing data (here, 40%) were excluded. Here, only the year 2018 was considered in the evaluation because of their data availability and adequacy after data checking (>60%) during the beginning of the study (Table 1).

Table 1. TMD gauges used for precipitation comparison.

Station	Province	Type	Adequacy	Period
Bang Na (BN) WMO: 484530	Bangkok	SG (3 hourly)	93.2%	Nov. 2017 to Oct. 2018
		AWS (10 min.)	87.1%	
Kampaeng Saen (KS) WMO: 484510	Nakhon Pathom	SG (3 hourly)	92.1%	
		AWS (10 min.)	86.8%	
Pathum Thani (PT) WMO: 484190	Pathum Thani	SG (3 hourly)	91.7%	
		AWS (10 min.)	61.3%	

3.2 Satellite precipitation

The satellite precipitation data used is GPM IMERG (shortly, GPM). The term IMERG stands for Integrated Multi–satellitE Retrievals for GPM), which is the algorithm that estimates precipitation by combining information from the GPM satellite constellation (qausi)-globally. The GPM mission is the successor of the Tropical Rainfall Measuring Mission (TRMM) conducted by the National Aeronautics and Space Administration (NASA) and the Japanese Aerospace Exploration Agency (JAXA) as well as other space agencies that launched the GPM Core Observatory satellite in 2014 [16-17, 28]. The GPM Core Observatory contains an advanced rain–sensing package, which includes an active radar to provide information on precipitation particles, layer–by–layer, within clouds, and a passive microwave imager to sense total precipitation within all cloud layers. The GPM mission's contributions have been acknowledged as bringing benefits to scientific and operational communities and the society in improving the understanding of water and energy cycles and the early waring or forecasting of extreme events. Three GPM versions (early, late run, and final run) are available. The first two versions are of near real–time production, with a latency of 4 h and 12 h, respectively. The final run is the most robust gauge–adjusted version, with a latency of 3.5 months and recommended for research [28], which was adopted in this study. Specifically, the full name of the data product utilized here is GPM IMERG Final Precipitation L3 Half Hourly 0.1°×0.1° (version 6), offering precipitation estimates back to mid–2000 (available at https://disc.gsfc.nasa.gov/datasets/GPM_3IMERGHH_06/summary). The full period of our study is 18 seasonal years (2001–2018), spanning November 2000 to October 2018. The definition of seasonal year is simply described as follows: For example, the seasonal year 2001 starts in November 2000 and ends in October 2001. The winter, summer and wet seasons of the year 2001 cover November 2000 to February 2001, March–April 2001, and May–October 2001, respectively. The full 18–year periods were divided to two 9–year epochs for precipitation comparison between the past and recent years: EP1 (2001–2009) and EP2 (2010–2018). It is noted that the product reports accumulated precipitation at the starting time of every half–hour". Thus, necessary adjustment was made to convert the original half–hourly data to hourly accumulated precipitation as reported at the end of hour to be consistent with the gauge data.

Three statistical metrics were employed to evaluate the accuracy of GPM estimates, which are correlation (*r*), normalized mean bias *(NMB*), and normalized mean error (*NME*). Correlation coefficient (r) measures the degree of linear association between two variables. *NMB* and *NME* determine the generic and absolute differences between the predicted and observed quantities, relative to the latter [15]. They are mathematically expressed as follows:

$$r = \frac{\sum_{i=1}^{n}(P_i-\bar{P})(O_i-\bar{O})}{\sqrt{\sum_{i=1}^{n}(P_i-\bar{P})^2\sum_{i=1}^{n}(O_i-\bar{O})^2}}, \quad (1)$$

$$NMB = \frac{\sum_{i=1}^{n}(P_i-O_i)}{\sum_{i=1}^{n}O_i}\times 100\%, \text{ and} \quad (2)$$

$$NME = \frac{\sum_{i=1}^{n}|P_i-O_i|}{\sum_{i=1}^{n}O_i}\times 100\%, \quad (3)$$

where P_i and O_i are the i^{th} prediction and observation, respectively, $\bar{P}$ and $\bar{O}$ are the prediction and observation means, respectively, and *n* is the number of data pairs.

3.3 Meteorological data

The National Centers for Environmental Prediction (NCEP)'s Climate Forecast System (CFS) reanalysis data were used to provide temperature and wind data at hourly and 0.5° resolutions (Table 2). Two versions are available: version 1 (CFSR) covering 1979–2010 [29] and version 2 (CFSv2) covering since 2011 [30] (available at https://rda.ucar.edu).

Table 2. List of the data used in the study.

Variable	Source	Resolution	Frequency	Years (calendar)
Precipitation	GPM IMERG (NASA)	0.1°	Half–hourly	2000–2018
Land cover	ESA CCI	0.00278°	Yearly	2002–2018
2–m Temperature (K) 850–mb Wind (m s^{-1}) 10–m Wind (m s^{-1})	CFS (NCEP/NOAA)	0.5°	Hourly	2000–2018

Remark:
GPM: Global Precipitation Measurement
NASA: National Aeronautics and Space Administration
ESA CCI: European Space Agency Climate Change Initiative
CFS: Climate Forecast System
NCEP/NOAA: National Centers for Environmental Prediction/National Oceanic and Atmospheric Administration, US

3.4 Land cover

Satellite–derived yearly land cover data from the European Space Agency Climate Change Initiative (ESA CCI) [27] were adopted for use (available at http://www.esa–landcover–cci.org), which have a 300–m resolution and 22 classes based on the classification of the Food and Agriculture Organization (FAO). This land cover product was developed using images from multiple satellites: Advanced Very–High–Resolution Radiometer (AVHRR) for 1992–1999, SPOT–Vegetation (SPOT–VGT) for 1998–2012, and PROBA–Vegetation (PROBA–V) and Sentinel–3 OLCI (S3 OLCI) for 2013–2019.

3.5 Grids

To support the work, four grids were defined, which are full domain (FD), Central Thailand (CT), GBK, and urban core (UC). The FD grid is only for general mapping. The grid resolutions (i.e., pixel or grid–cell sizes) and sizes of these four grids are given in Table 3 and Figure 3. The UC grid represents the urban core of GBK, for which urbanized (i.e., built–up) areas are still dominant, whose size was determined as follows: A site (13.75° Lat. and 100.56° Lon.) is marked as the city center. Next, the percentage of total urban areas found in the land–cover (ESA CCI) data is computed within a box with varying size (number of 300–m pixels per size = 1, 3, 5, 7, 9, …, and so on sequentially) and drawn (Figure 4). A sharp decline in total urban areas is first found at the box size of 31×31 pixels, then designated as UC. The box size is approximately equivalent to 9×9 km^2 and a single one GPM pixel. As seen from the table and the figure, the urban areas in the UC grid does not change much over time (e.g., 2005 and 2015) and is reasonably robust for use over the full period.

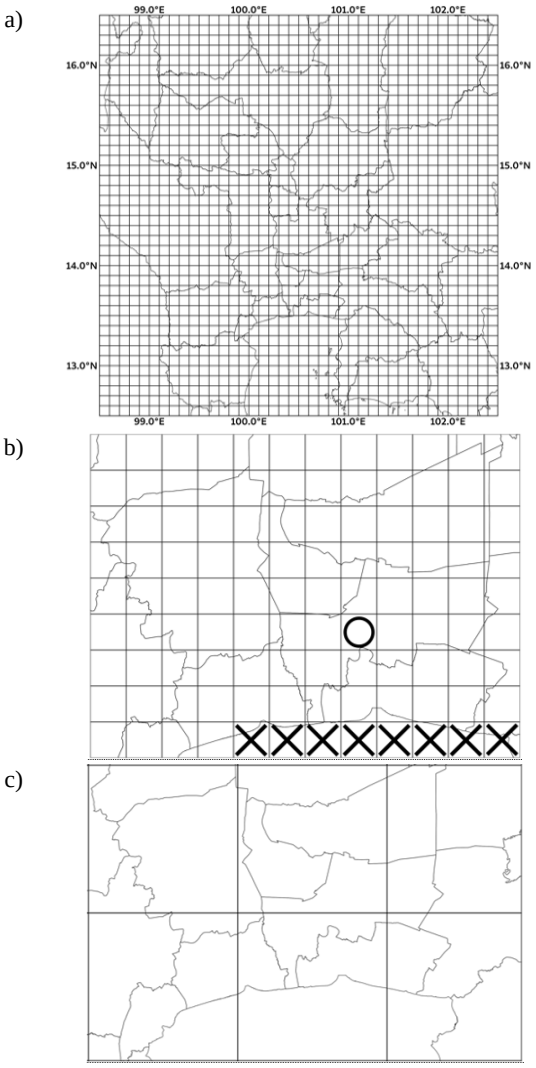

Figure 3. a) GPM grid over the full domain, b) GPM grid for GBK, and c) MET–GBK. In c), the circle and crosses marks the urban core (UC) and the non-land pixels (excluded in calculation).

Table 3. Grids considered in the study.

Grid	Pixels	Resolution	Urban (%) in 2005	Urban (%) in 2015
Full domain (FD)	40×40	0.1˚	0.73	1.33
Greater Bangkok (GBK)	12×9	0.1˚	7.71	12.39
Urban core (UC)	1×1	0.1˚	96.08	98.45
Meteorological (MET–GBK)	9×9	0.5˚	NA	NA

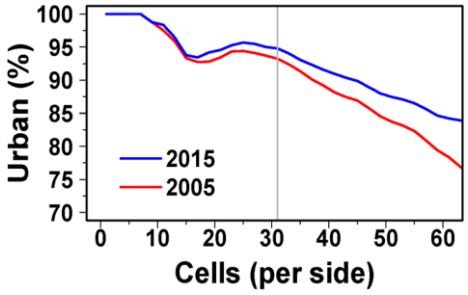

Figure 4. Total urban area (%) versus the size of a UC–centered box in units of land–cover (ESA CCI) pixels. Here, a box of 31×31 pixels is shown to properly represent UC.

4. Results and Discussion

4.1 GPM performance

Figure 5 displays comparison between the standard–gauge (SG) and automatic–gauge (AWS) data for 3–hourly precipitation, showing reasonable agreement with $r > 0.8$, *NMB* (in magnitude) < 20% and *NME* < 50% at all three stations. However, AWS appears to have a technical problem of occasionally reporting very low values while SG, which is the most reliable, does not. For GPM with AWS for hourly precipitation, relatively poor agreement is seen. Nevertheless, correlation, though low, is still positive ($r < 0.3$) with both NMB and NMB being within 100% (*NMB* = 44%–59% and *NME* = 88%–98%) The GPM data are satellite–based and of pixel–wise average (0.1° resolution or about 10 km) while the gauges are point–wise, which is incompatible by nature of spatial representation.

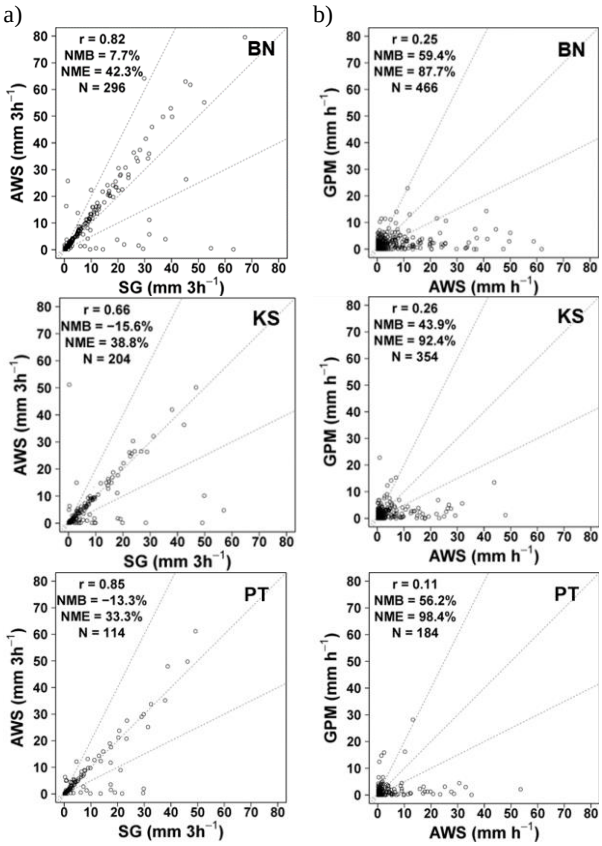

Figure 5. Comparison of a) 3–hourly precipitation (SG vs AWS) and b) hourly precipitation (AWS vs GPM). A threshold of <0.1 mm (i.e., trace amount) was necessarily applied here to screening out the data before comparison to avoid the irregular systematic presence of zero values in the AWS data.

4.2 Seasonal and diurnal variations

Over GBK, monthly precipitation by GPM well captures seasonality with two peaks in the early and late wet season (for both average and extreme) (Figure 6 and Figure S2 in Supplementary Materials). Temperature also does so, being the highest in April and relatively low in the winter. As seen, the winter has quite a limited amount of precipitation and is considered not important. In the following, only precipitation in the summer and the wet-season is given attention to. Monthly pattern varies year–to–year but the seasonality is maintained as governed by the two regional monsoons (Figure 7a). For diurnal variation, summer precipitation tends to occur in the afternoon and evening, so does wet–season precipitation, but extended to the early morning hours and with higher intensity in the evening (Figure 7b). These timings suggest enhanced convection by solar radiation.

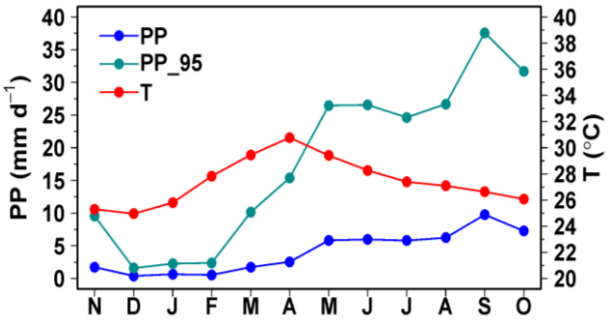

Figure 6. Monthly precipitation and temperature in GBK over 2001–2018. PP is the average precipitation, PP_95 is the extreme (95th percentile) precipitation, and T is the average temperature. The *x*–axis labels correspond to the following months of year (November, December, January, …, and October).

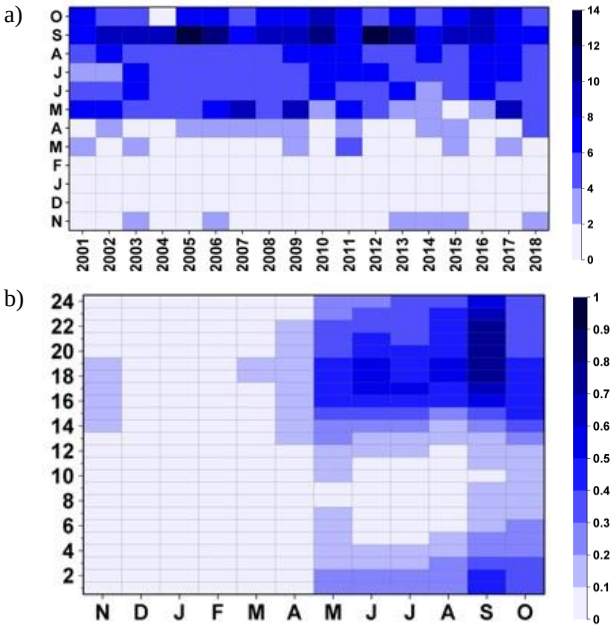

Figure 7. a) Monthly precipitation by year (mm d^{-1}) and b) hourly precipitation by month (mm h^{-1}) in GBK during 2001–2018.

4.3 Spatial homogeneity

Given that our focused study area is GBK, it is thus of further interest to assure whether GBK represents itself as one single homogeneous region in terms of hourly precipitation. If so, comparison of precipitation in urban and non–urban areas can be directly made and discussed in a robust fashion. In doing so, spatial correlation of hourly precipitation at UC and its surround pixels was computed pixel–wise (Figure 8). As seen, correlation declines with distance from UC but areas with high correlation (>0.6) are mostly to UC, suggesting the possibility to consider GBK as the well–defined or coherent region of hourly precipitation in support of further investigation.

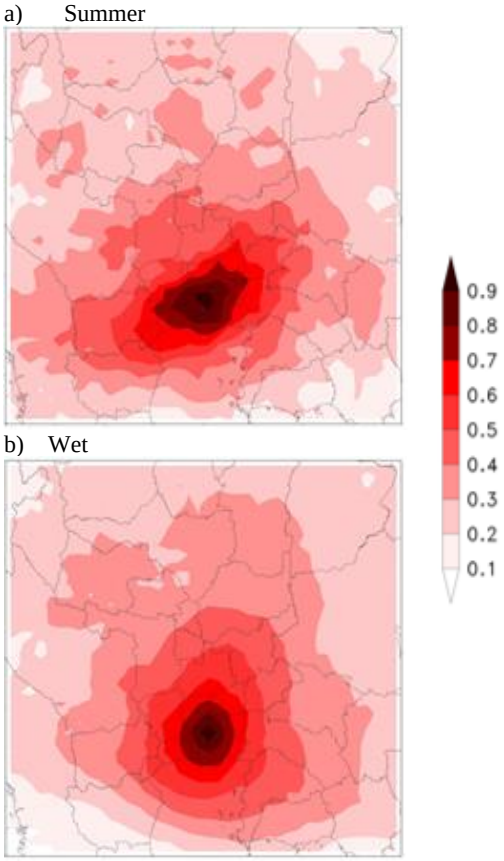

Figure 8. Seasonal maps of correlation of hourly precipitation between UC and its surrounding areas.

4.4 Urban and non–urban precipitation

In this section, all GBK pixels were grouped into two classes (urban and non–urban), and class–wise quantities were computed. Figure 9 compares urban and non–urban precipitation by quantity and season. In three of four case (summer average, wet–season average, and wet–season extreme), urban precipitation is larger than its non–urban counterpart. This suggests that urban surface and city activities possibly enhance more convection, as compared to the non–urban areas. Moreover, urban precipitation in all four cases appears to be more concentrated (i.e., less spreading or distributed). However, the mean differences are statistically significant only in the wet season using a Wilcoxon rank–sum test. Both summer average and extreme precipitation appear to be in the same order of magnitude (within 0.5 mm h^{-1}), with their mean differences between the two classes being insignificant. For the wet season, extreme precipitation is obviously much larger. Given relatively abundant moisture in this season, urban surface and city activities act to amplify precipitation more apparently.

Advection (i.e., wind) can transport moisture and convective cells from one place to another. Precipitation taking place away from the city center is expected to be directionally dependent [5, 10]. Here, a matrix of 7×7 GPM pixels (centered at UC) was employed (Figure 10), and precipitation amounts averaged over pixels along the standard eight directions were compared to that in UC (Table 4). Considering both average and extreme quantities in the summer, areas surrounding UC in the north, northeast, and east tend to have larger precipitation, which corresponds to the surface and upper winds prevailing towards these directions during this season (Figure 11) and also carrying moisture from

the Gulf of Thailand, located south of GBK. However, the wet season does not have such directional contrast because moisture is well present and temperature is not as high as in the summer. Also, more precipitation makes urban surface become wetter, reducing sensible heat to air and in turn convection. These are some potential factors for the lesser directional dependence observed in the wet season. A sensitivity test was additionally performed by assigning the cells of the 7×7 matrix with slightly different directions, and the general finding said above fairly holds (see Figure S3 and Table S1 in Supplementary Materials).

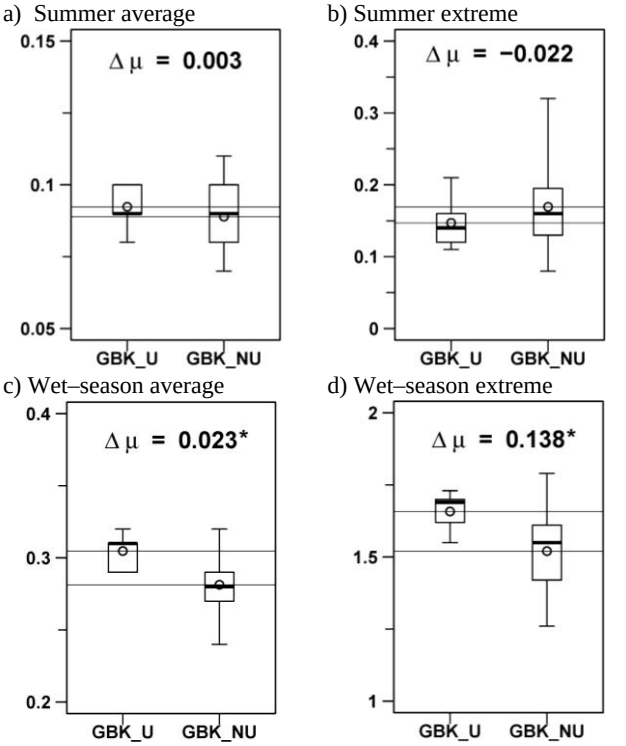

Figure 9. Distributions of urban (U) and non–urban (NU) precipitation (mm h^{-1}) over GBK by quantity (i.e., average and extreme) and season (i.e., summer and wet). Each box–whisker shows the distribution values pooled from all pixels (corresponding to U or NU), in which the circle denotes the mean, the top and bottom dashes are the maximum and minimum, respectively, and the top, middle, and bottom lines of the box are the 75th, 50th, and 25th percentiles, respectively. $\Delta\mu$ is the mean difference of urban and non–urban precipitation, marked by an asterisk for statistical significance at a 0.05 level.

NW	NW	NW	N	NE	NE	NE
NW	NW	NW	N	NE	NE	NE
NW	NW	NW	N	NE	NE	NE
W	W	W	**UC**	E	E	E
SW	SW	SW	S	SE	SE	SE
SW	SW	SW	S	SE	SE	SE
SW	SW	SW	S	SE	SE	SE

Figure 10. Matrix to examine the directional dependence of precipitation. The letters N, NE, E, …, W, and NW are the standard eight directions around UC (clockwise from north to northwest).

Table 4. Direction–wise precipitation (mm d^{-1}) around UC.

Direction	Average	
	Summer	**Wet**
NW	2.15	6.81
N	2.28	6.99
NE	**2.33 (+1.2%)**	7.13
W	2.19	7.11
UC	2.30	7.23
E	2.31	7.28
SW	2.20	7.03
S	2.28	7.11
SE	2.32	7.25
Direction	**Extreme**	
	Summer	**Wet**
NW	13.55	29.58
N	**15.51 (+4.5%)**	29.54
NE	**15.61 (+5.2%)**	30.15
W	13.57	30.26
UC	14.84	31.26
E	**15.69 (+5.7%)**	30.83
SW	13.80	30.86
S	14.51	31.20
SE	**15.28 (+3.0%)**	**31.65 (+1.2%)**

Remark: The bold numbers mark the directions along which precipitation is larger than UC (by 1% at least), and the parenthesized values are the corresponding differences.

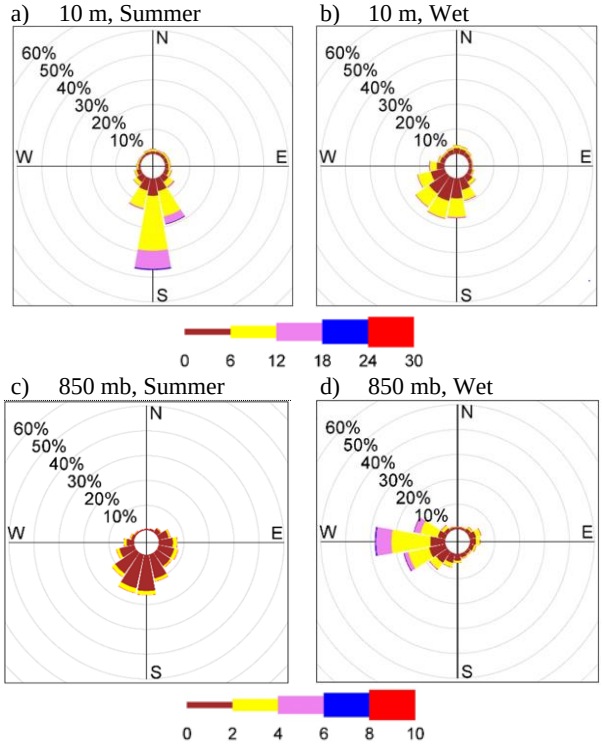

Figure 11. Wind roses at 10 m agl and 850 mb by season. The units of wind are m s^{-1}.

4.5 Urbanization effects

To investigate how urbanization affects precipitation, the urban and non–urban classes for GBK observed in the years 2005 and 2015 were representatively used for the past and recent epochs (see Section 3.2), i.e., EP1 (2001–2009) and EP2 (2010–2018). The urban areas found over GBK in 2005 and 2015 are 7.7% and 12.4%. The monthly and diurnal variations of precipitation found in each class in each epoch were plotted as Hovmoller diagrams (Figures 12). Only the summer and wet seasons are considered since the winter has very limited precipitation. In the figure, precipitation was normalized by total

precipitation from both classes, which is necessary to avoid a bias induced by different amounts of precipitation in the two epochs. For any paired month (of year) and hour (of day), the sum of urban and non–urban precipitation amounts equals 100%. The two bottom plots in the figure shows final changes in normalized precipitation between the two epochs for the urban and non–urban areas, respectively. It is seen that March–May has relatively large changes in magnitude (i.e., more fluctuation) than those the other months. During the summer, such large changes tend to occur mostly in the afternoon and evening/nighttime. The changes however do not show a systematic pattern to point conclusively to whether urbanization induces more or less precipitation for this case study, which is perhaps partly explained by the fact that the urbanization in GBK between 2005 and 2015 is not large (i.e. 4.7%).

5. Conclusions

Several precipitation characteristics in Greater Bangkok (GBK) were investigated using the hourly GPM precipitation estimates for 2001–2018 (as seasonal years). Long–term land cover and meteorological data were also used to support the work. The GPM data was compared using hourly gauge data, having somewhat low but positive correlation with bias and error within practical thresholds. GPM well captures seasonality, with two peaks in the early and late wet season, as regulated by the meridional migration of the monsoon trough. On the diurnal scale, summer precipitation tends to occur during the afternoon and evening, so does wet–season precipitation, but extended to the early morning hours. These timings suggest enhanced convection by solar radiation. Spatial correlation analysis using hourly data indicates GBK as a homogeneous region of precipitation sufficiently for both summer and wet season. Urban precipitation tends to be larger and less distributed than its non–urban counterpart, suggesting that urban surface and city activities possibly enhance more convection. Wind can also transport moisture and convective cells. It was found that precipitation shows strong directional dependence in the summer, consistent with the prevailing surface and upper winds. As for urbanization effect, it was examined using a set of Hovmoller diagrams for summer and wet–season precipitation in GBK and comparing normalized precipitation in the urban and non–urban areas between two epochs (2001–2009 and 2010–2018). It was found that March–May has relatively large changes in magnitude than those the other months. In the summer, such changes tend to occur mostly in the afternoon and evening/nighttime. It is however not possible to conclude from the results and beyond the scope of this study for whether urbanization induces more or less precipitation in GBK.

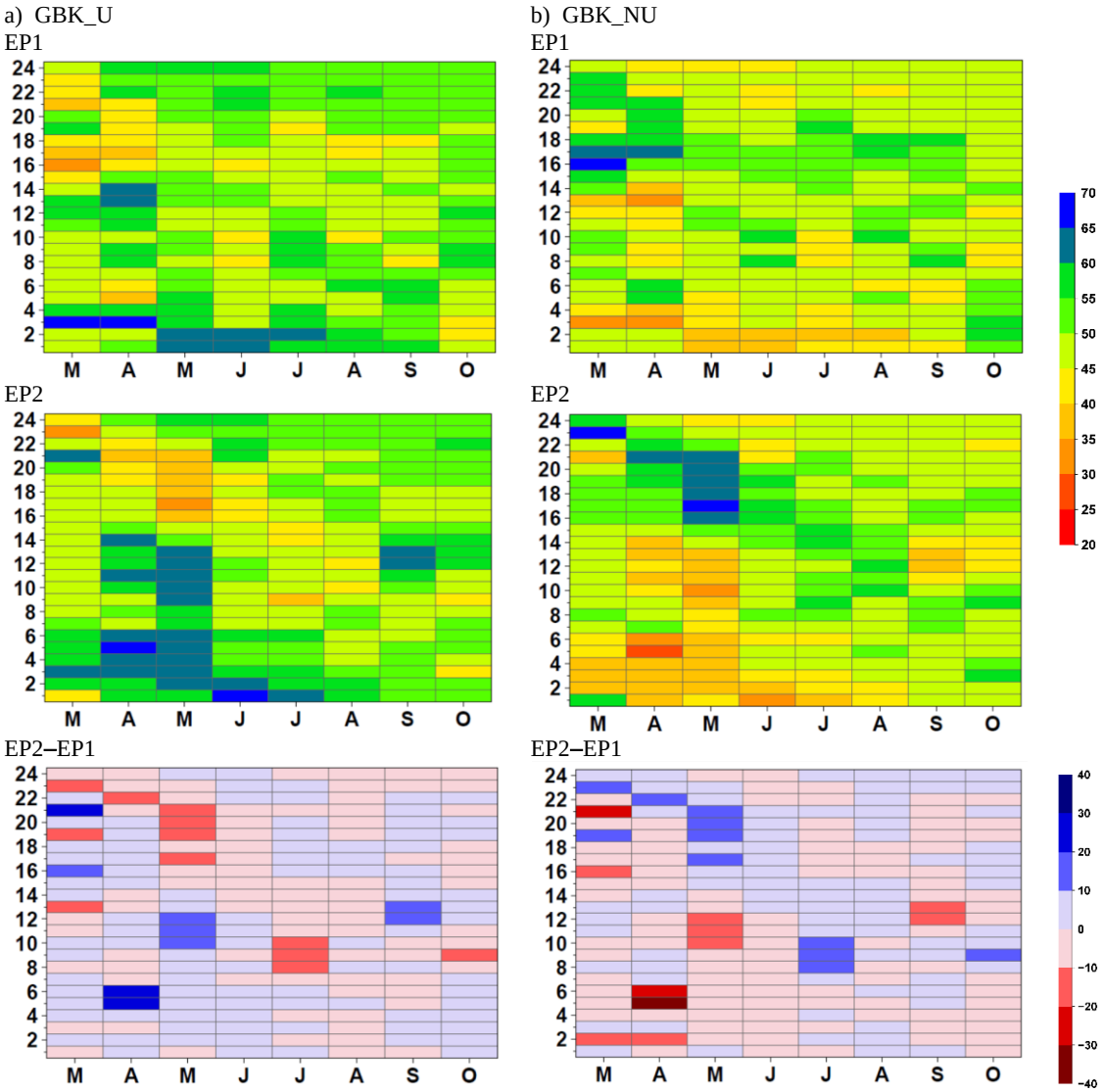

Figure 12. Normalized precipitation over hours of day in the urban and non–urban areas in GBK during the two epochs and their difference.

This present study has a number of limitations, upon which future work may improve. They are listed and suggested as follows: Bias correction with data from a dense gauge network, if accessible, on satellite precipitation can be useful to help reduce errors or uncertainty in estimates. Use of different satellite precipitation products or even weather radar can offer additional perspectives on uncertainty in the spatiotemporal variation of precipitation. The gridded land cover data used here should be inspected with local data if available. Apart from intensity, other precipitation characteristics that may be impacted by urbanization, should also be examined, e.g., frequency, duration, and extreme events. Lastly, precipitation is complex natural process, and its numerical modeling is beneficial to support investigating the potential impacts of urbanization as well as urban pollution.

Acknowledgements

The authors thank the Thai Meteorology Department (TMD) for the surface monitoring data. We also thank Dr. Surajate Boonya–aroonnet and an anonymous reviewer for their useful comments. This study was supported by the Joint Graduate School of Energy and Environment (JGSEE), the Postgraduate Education and Research Development Organization (PERDO), the Hydro–Informatics Institute (HII), and the Energy Conservation and Promotion Fund (ENCONFUND) of the Ministry of Energy.

Conflicts of Interest

The authors declare no conflict of interest.

Supplementary Materials

The supplement information of this article is available at http://www.jseejournal.com.

References

[1] Qin, Y., Chen, Z., Shen, Y., Zhang, S. and Shi, R. 2014. Evaluation of satellite rainfall estimates over the Chinese Mainland, *Remote Sensing*, 6, 11649-11672.

[2] Gebremichael, M. and Hossain, F. (Editors) 2010. *Satellite Rainfall Applications for Surface Hydrology*, Springer.

[3] Zhang, Y., Smith, J.A., Luo, L., Wang, Z. and Baeck, M.L. 2014. Urbanization and rainfall variability in the Beijing Metropolitan Region, *Journal of Hydrometeorology*, 15, 2219-2235.

[4] Mahmoud, M.T., Hamouda, M.A. and Mohamed, M.M. 2019. Spatiotemporal evaluation of the GPM satellite precipitation products over the United Arab Emirates, *Atmospheric Research*, 219, 200-212.

[5] McLeod, J., Shepherd, M. and Konrad, C.E. 2017. Spatio–temporal rainfall patterns around Atlanta, Georgia and possible relationships to urban land cover, *Urban Climate*, 21, 27-42.

[6] Han, J.Y., Baik, J.J. and Lee, H. 2014. Urban impacts on precipitation, *Asia–Pacific Journal of Atmospheric Sciences*, 50, 17-30.

[7] Paton, C. and Manomaiphiboon, K. 2013. A metropolitan wind resource assessment for Bangkok, Thailand part 1: Wind resource mapping, *Journal of Sustainable Energy and Environment*, 4, 69-76.

[8] Kamma, J., Manomaiphiboon, K., Aman, N., Thongkamdee, T., Chuangchote, S. and Bonnet, S. 2020. Urban heat island analysis for Bangkok: Multi–scale temporal variation, associated factors, directional dependence, and cool island condition, *ScienceAsia*, 46, 213-223.

[9] Pakarnseree, R., Chunkao, K. and Bualert, S. 2018. Physical characteristics of Bangkok and its urban heat island phenomenon, *Building and Environment*, 143, 561-569.

[10] Shepherd, J.M., Pierce, H. and Negri, A.J. 2002. Rainfall modification by major urban areas: Observations from spaceborne rain radar on the TRMM satellite, *Journal of Applied Meteorology*, 41, 689-701.

[11] Chen, S., Li, W.B., Du, Y.D., Mao, C.Y. and Zhang, L. 2015. Urbanization effect on precipitation over the Pearl River Delta based on CMORPH data, *Advances in Climate Change Research*, 6, 16-22.

[12] Wang, D., Jiang, P., Wang, G. and Wang, D. 2015. Urban extent enhances extreme precipitation over the Pearl River Delta, China, *Atmospheric Science Letters*, 16, 310-317.

[13] Abiola, S.F., Mohd–Mokhtar, R., Ismail, W., Mohamad, N. and Mandeep, J.S. 2011. Satellite and ground data rainfall characterization in Malaysia, *2011 IEEE International Conference on Space Science and Communication (IconSpace)*, Penang, Malaysia.

[14] Satgé, F., Bonnet, M.-P., Gosset, M., Molina, J., Lima, W.H.Y., Zolá, R.P., Timouk, F. and Garnier, J. 2016. Assessment of satellite rainfall products over the Andean plateau, *Atmospheric Research*, 167, 1-14.

[15] Hoang, T.T., Manomaiphiboon, K., Singhrattna, N. and Assareh, N. 2020. Evaluation of multiple sub–daily satellite precipitation products for Thailand, *Journal of Sustainable Energy and Environment*, 11, 81-91.

[16] Hou, A.Y., Kakar, R.K., Neeck, S., Azarbarzin, A.A., Kummerow, C.D., Kojima, M., Oki, R., Nakamura, K. and Iguchi, T. 2014. The Global Precipitation Measurement mission, *Bulletin of the American Meteorological Society*, 95, 701-722.

[17] Skofronick–Jackson, G., Petersen, W.A., Berg, W., Kidd, C., Stocker, E.F., Kirschbaum, D.B., Kakar, R., Braun, S.A., Huffman, G.J., Iguchi, T., Kirstetter, P.E., Kummerow, C., Meneghini, R., Oki, R., Olson, W.S., Takayabu, Y.N., Furukawa, K. and Wilheit, T. 2017. The Global Precipitation Measurement (GPM) mission for science and society, *Bulletin of the American Meteorological Society*, 98, 1679-1695.

[18] Kachenchart, B., Kamlangkla, C., Puttanapong N. and Limsakul, A. 2021. Urbanization effects on surface air temperature trends in Thailand during 1970–2019, *Environmental Engineering Research*, 26, 200378, doi: https://doi.org/10.4491/eer.2020.378.

[19] Kirtphaiboon, S., Wongwises, P., Limsakul, A., Sooktawee, S. and Humphries, U. 2014. Rainfall variability over Thailand related to the El Nino–Southern Oscillation (ENSO), *Journal of Sustainable Energy and Environment*, 5, 17-30.

[20] Sarinnapakorn, K., Thodsan, T., Torsi, K., Boonya–Aroonnet, S. and Qin, X. 2016. Numerical simulation of Bangkok heavy rainfall with urbanization effects, *International Conference on Sustainable Energy and Environment (SEE2016) in conjunction with 1st International Conference on Climate Technology and Innovation (CTI2016)*, (pp. 549-552). 28–30 November 2016, Dusit Thani Hotel, Bangkok, Thailand.

[21] Torsri, K., Octaviani, M., Manomaiphiboon, K. and Towprayoon, S. 2013. Regional mean and variability characteristics of temperature and precipitation over Thailand in 1961–2000 by a regional climate model and their evaluation, *Theoretical and Applied Climatology*, 113, 289-304.

[22] TMD. 2015. *Climate of Thailand*. Thai Meteorological Department. Available online: https://www.tmd.go.th/en/archive/thailand_climate.pdf [Accessed on: 19 November 2019].

[23] TMD. 2008. *Automatic Weather System*. Thai Meteorological Department. Available online: http://www.aws–

observation.tmd.go.th/web/reports/weather_minute.asp [Accessed on: 19 November 2019].

[24] NSO. 2020. *Gross Provincial Product for Thailand*. Greater Bangkok, and Bangkok, National Statistical Office. Available online: http://service.nso.go.th/nso/web/statseries/statseries15.html [Accessed on: 23 September 2020].

[25] EPPO. 2020. *Total Energy Consumption*. Energy Policy and Planning Office. Available online: https://data.energy.go.th/output/consumption/search [Accessed on: 23 September 2020].

[26] NSO. 2020. *Registered Population for Thailand, Greater Bangkok, and Bangkok*. National Statistical Office. Available online: http://statbbi.nso.go.th/staticreport/page/sector/en/01.aspx [Accessed on: 23 September 2020].

[27] ESA CCI. 2020. *Land Cover Classification Gridded Maps from 1992 to Present Derived from Satellite Observations, Demographic and Home Data*. European Space Agency (Climate Change Initiative). Available online: https://www.copernicus.eu/lt/node/9461 [Accessed on: 23 September 2020].

[28] Huffman, G.J., Bolvin, D.T., Braithwaite, D., Hsu, K., Joyce, R., Kidd, C., Nelkin, E.J., Sorooshian, S., Tan, J. and Xie, P. 2019. *Algorithm Theoretical Basis Document (ATBD) Version 06, NASA Global Precipitation Measurement (GPM) Integrated Multi–satellite Retrievals for GPM (IMERG)*. National Aeronautics and Space Administration. Available online: https://docserver.gesdisc.eosdis.nasa.gov/public/project/GPM/IMERG_ATBD_V06.pdf [Accessed on: 19 November 2019].

[29] Saha, S., Moorthi, S., Pan, H.L., Wu, X., Wang, J., Nadiga, S., Tripp, P., Kistler, R., Woollen, J., Behringer, D., Liu, H., Stokes, D., Grumbine, R., Gayno, G., Wang, J., Hou, Y.T., Chuang, H.Y., Juang, H.M.H., Sela, J., Iredell, M., Treadon, R., Kleist, D., Delst, P.V., Keyser, D., Derber, J., Ek, M., Meng, J., Wei, H., Yang, R., Lord, S., Dool, H.V.D., Kumar, A., Wang, W., Long, C., Chelliah, M., Xue, Y., Huang, B., Schemm, J.K., Ebisuzaki, W., Lin, R., Xie, P., Chen, M., Zhou, S., Higgins, W., Zou, C.Z., Liu, Q., Chen, Y., Han, Y., Cucurull, L., Reynolds, R.W., Rutledge, G. and Goldberg, M. 2010. The NCEP Climate Forecast System Reanalysis, *Bulletin of the American Meteorological Society*, 91, 1015-1058.

[30] Saha, S., Moorthi, S., Wu, X., Wang, J., Nadiga, S., Tripp, P., Behringer, D., Hou, Y.T., Chuang, H.Y., Iredell, M., Ek, M., Meng, J., Yang, R., Mendez, M.P., Dool, V.D., Zhang, Q., Wang, W., Chen, M. and Becker, E. 2014. The NCEP climate forecast system version 2, *Journal of Climate*, 27, 2185-2208.

Supplementary Materials

Satellite precipitation characteristics and effects of land cover change in Greater Bangkok

Chankasem et al.

a) b)

Figure S1. a) Standard gauge and b) auto gauge at the Bang–Na weather station of the TMD.

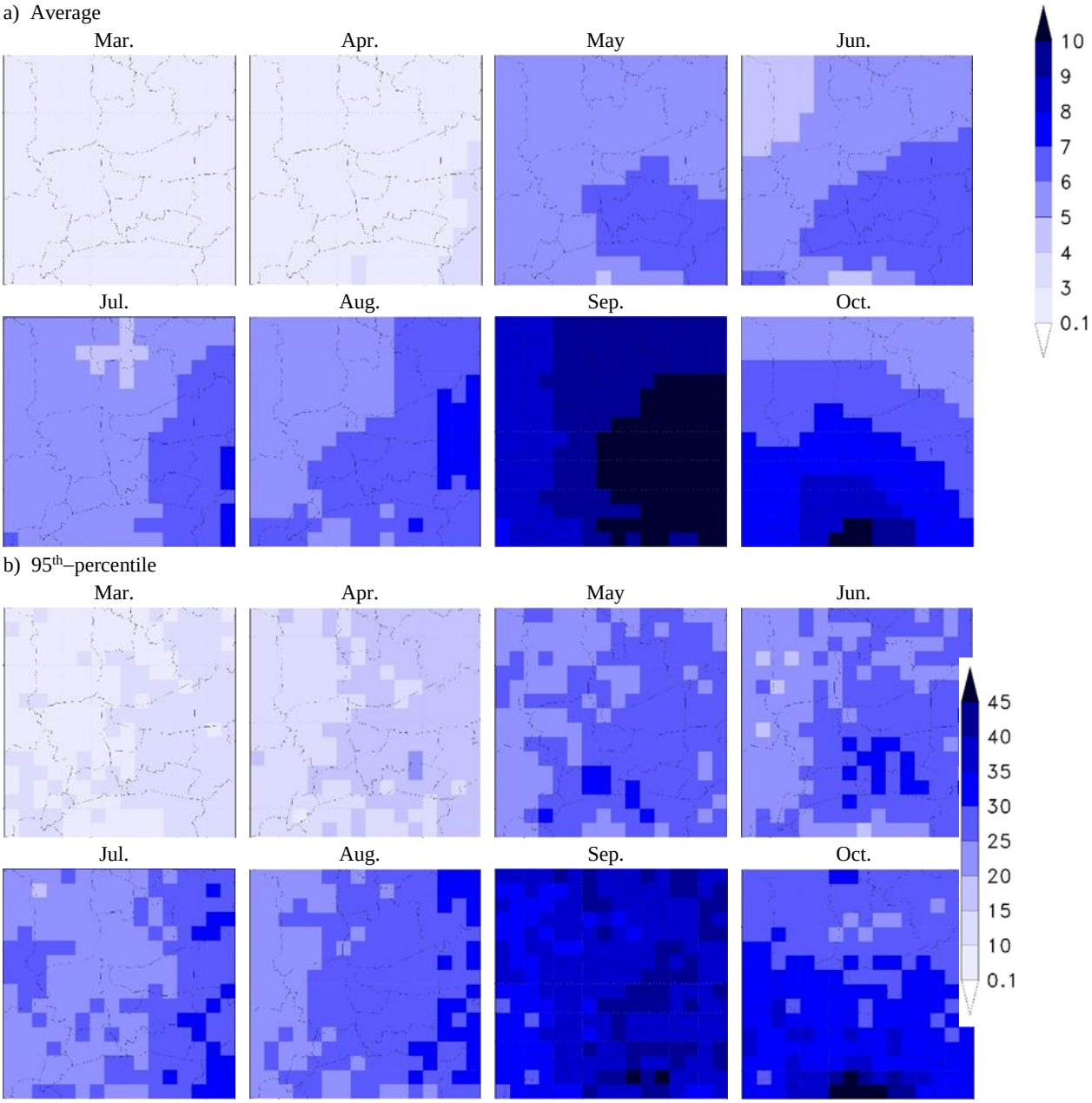

Figure S2. a) Monthly precipitation (mm d^{-1}) and b) Monthly 95th–percentile precipitation (mm d^{-1}) over GBK.

NW	NW	N	N	N	NE	NE
NW	NW	NW	N	NE	NE	NE
W	NW	NW	N	NE	NE	E
W	W	W	**UC**	E	E	E
W	SW	SW	S	SE	SE	E
SW	SW	SW	S	SE	SE	SE
SW	SW	S	S	S	SE	SE

Figure S3 Matrix to examine the directional dependence of precipitation. The letters N, NE, E, …, W, and NW are the standard eight directions around UC (clockwise from north to northwest).

Table S1 Direction–wise precipitation (mm d^{-1}) around UC.

Direction	Average		Extreme	
	Summer	Wet	Summer	Wet
NW	2.14	6.81	13.60	29.68
N	2.26	6.92	14.87	29.29
NE	**2.34 (+1.6%)**	7.14	**15.99 (+7.7%)**	30.27
W	2.17	7.05	13.29	30.00
Urban Core	2.30	7.23	14.84	31.26
E	2.30	7.29	**15.36 (+3.5%)**	30.76
SW	2.21	7.04	13.75	31.15
S	2.26	7.08	14.55	31.27
SE	**2.33 (+1.3%)**	7.26	**15.48 (+4.3%)**	**31.62 (+1.2%)**

Remark:
The bold numbers mark the directions along which precipitation is larger than UC (by 1% at least), and the parenthesized values are the corresponding differences.